In conclusion, we found that an examination of only the 16 central points of the HFA 10-2 test shortened testing time and correlated well with both the average HFA 10-2 TD (16 central test points) and the OCT-measured retinal macular layer thickness. A small stimulus size also helped improve the sensitivity of the evaluation of macular function. This macular sectorial approach can likely improve the accuracy of examinations of glaucoma patients with decreased macular function.

Acknowledgments The authors thank Mr Yukihiro Shiga and Mr Ryou Watanabe for data acquisition, and Mr Tim Hilts for editing of this manuscript.

References

1. Quigley HA. Number of people with glaucoma worldwide. Br J Ophthalmol. 1996;80:389–93.
2. Quigley HA, Dunkelberger GR, Green WR. Retinal ganglion cell atrophy correlated with automated perimetry in human eyes with glaucoma. Am J Ophthalmol. 1989;107:453–64.
3. Heijl A, Leske MC, Bengtsson B, Hyman L, Hussein M. Reduction of intraocular pressure and glaucoma progression: results from the Early Manifest Glaucoma Trial. Arch Ophthalmol. 2002;120:1268–79.
4. Kass MA, Heuer DK, Higginbotham EJ, Johnson CA, Keltner JL, Miller JP, et al. The Ocular Hypertension Treatment Study: a randomized trial determines that topical ocular hypotensive medication delays or prevents the onset of primary open-angle glaucoma. Arch Ophthalmol. 2002;120:701–13 (discussion 829–30).
5. Quigley HA, Broman AT. The number of people with glaucoma worldwide in 2010 and 2020. Br J Ophthalmol. 2006;90:262–7.
6. Iwase A, Suzuki Y, Araie M, Yamamoto T, Abe H, Shirato S, et al. The prevalence of primary open-angle glaucoma in Japanese: the Tajimi Study. Ophthalmology. 2004;111:1641–8.
7. Kim CS, Seong GJ, Lee NH, Song KC. Prevalence of primary open-angle glaucoma in central South Korea: the Namil study. Ophthalmology. 2011;118:1024–30.
8. Liang YB, Friedman DS, Zhou Q, Yang X, Sun LP, Guo LX, et al. Prevalence of primary open angle glaucoma in a rural adult Chinese population: the Handan eye study. Invest Ophthalmol Vis Sci. 2011;52:8250–7.
9. Araie M, Arai M, Koseki N, Suzuki Y. Influence of myopic refraction on visual field defects in normal tension and primary open angle glaucoma. Jpn J Ophthalmol. 1995;39:60–4.
10. Mayama C, Suzuki Y, Araie M, Ishida K, Akira T, Yamamoto T, et al. Myopia and advanced-stage open-angle glaucoma. Ophthalmology. 2002;109:2072–7.
11. Nakazawa T, Fuse N, Omodaka K, Aizawa N, Kuwahara S, Nishida K. Different types of optic disc shape in patients with advanced open-angle glaucoma. Jpn J Ophthalmol. 2010;54:291–5.
12. Omodaka K, Nakazawa T, Yokoyama Y, Doi H, Fuse N, Nishida K. Correlation between peripapillary macular fiber layer thickness and visual acuity in patients with open-angle glaucoma. Clin Ophthalmol. 2010;4:629–35.
13. Nicolela MT, Drance SM. Various glaucomatous optic nerve appearances: clinical correlations. Ophthalmology. 1996;103:640–9.
14. Nicolela MT, McCormick TA, Drance SM, Ferrier SN, LeBlanc RP, Chauhan BC. Visual field and optic disc progression in patients with different types of optic disc damage: a longitudinal prospective study. Ophthalmology. 2003;110:2178–84.
15. Sung KR, Cho JW, Lee S, Yun SC, Choi J, Na JH, et al. Characteristics of visual field progression in medically treated normal-tension glaucoma patients with unstable ocular perfusion pressure. Invest Ophthalmol Vis Sci. 2011;52:737–43.
16. Sumi I, Shirato S, Matsumoto S, Araie M. The relationship between visual disability and visual field in patients with glaucoma. Ophthalmology. 2003;110:332–9.
17. Huang D, Swanson EA, Lin CP, Schuman JS, Stinson WG, Chang W, et al. Optical coherence tomography. Science. 1991;254:1178–81.
18. Mwanza JC, Oakley JD, Budenz DL, Chang RT, Knight OJ, Feuer WJ. Macular ganglion cell-inner plexiform layer: automated detection and thickness reproducibility with spectral domain-optical coherence tomography in glaucoma. Invest Ophthalmol Vis Sci. 2011;52:8323–9.
19. Morooka S, Hangai M, Nukada M, Nakano N, Takayama K, Kimura Y, et al. Wide 3-dimensional macular ganglion cell complex imaging with spectral-domain optical coherence tomography in glaucoma. Invest Ophthalmol Vis Sci. 2012;53:4805–12.
20. Kim NR, Lee ES, Seong GJ, Kim JH, An HG, Kim CY. Structure-function relationship and diagnostic value of macular ganglion cell complex measurement using Fourier-domain OCT in glaucoma. Invest Ophthalmol Vis Sci. 2010;51:4646–51.
21. Seong M, Sung KR, Choi EH, Kang SY, Cho JW, Um TW, et al. Macular and peripapillary retinal nerve fiber layer measurements by spectral domain optical coherence tomography in normal-tension glaucoma. Invest Ophthalmol Vis Sci. 2010;51:1446–52.
22. Raza AS, Cho J, de Moraes CG, Wang M, Zhang X, Kardon RH, et al. Retinal ganglion cell layer thickness and local visual field sensitivity in glaucoma. Arch Ophthalmol. 2011;129:1529–36.
23. Sakamoto A, Hangai M, Nukada M, Nakanishi H, Mori S, Kotera Y, et al. Three-dimensional imaging of the macular retinal nerve fiber layer in glaucoma with spectral-domain optical coherence tomography. Invest Ophthalmol Vis Sci. 2010;51:5062–70.
24. Na JH, Kook MS, Lee Y, Baek S. Structure-function relationship of the macular visual field sensitivity and the ganglion cell complex thickness in glaucoma. Invest Ophthalmol Vis Sci. 2012;53:5044–51.
25. Kerrigan-Baumrind LA, Quigley HA, Pease ME, Kerrigan DF, Mitchell RS. Number of ganglion cells in glaucoma eyes compared with threshold visual field tests in the same persons. Invest Ophthalmol Vis Sci. 2000;41:741–8.
26. Drasdo N, Millican CL, Katholi CR, Curcio CA. The length of Henle fibers in the human retina and a model of ganglion receptive field density in the visual field. Vis Res. 2007;47:2901–11.
27. Kang SH, Hong SW, Im SK, Lee SH, Ahn MD. Effect of myopia on the thickness of the retinal nerve fiber layer measured by Cirrus HD optical coherence tomography. Invest Ophthalmol Vis Sci. 2010;51:4075–83.
28. Leung CK, Yu M, Weinreb RN, Ye C, Liu S, Lai G, et al. Retinal nerve fiber layer imaging with spectral-domain optical coherence tomography: a prospective analysis of age-related loss. Ophthalmology. 2012;119:731–7.

Journal of Neurochemistry

JOURNAL OF NEUROCHEMISTRY | 2013 | 127 | 669–680

doi: 10.1111/jnc.12325

ORIGINAL ARTICLE

Critical role of Nrf2 in oxidative stress-induced retinal ganglion cell death

Noriko Himori,* Kotaro Yamamoto,* Kazuichi Maruyama,* Morin Ryu,* Keiko Taguchi,† Masayuki Yamamoto† and Toru Nakazawa*

*Department of Ophthalmology, Tohoku University Graduate School of Medicine, Sendai, Miyagi, Japan

†Department of Medical Biochemistry, Tohoku University Graduate School of Medicine, Sendai, Miyagi, Japan

Abstract

NF-E2 related factor 2 (Nrf2) is a key transcription factor that plays a pivotal role in endogenous protection against oxidative stress. However, the role of Nrf2 in visual disorders remains unclear. It has been reported that oxidative stress is thought of as one of the causes of glaucoma. Here, we investigate whether the function of Nrf2 in oxidative stress-induced retinal ganglion cell (RGC) death. This study used adult male Nrf2 deficient mice (Nrf2 KO) and age- and sex-matched wild-type (WT) mice. We dissociated and purified *N*-4-[4-didecylaminostryryl]-*N*-methyl-pyridinium iodide-labeled RGCs with fluorescence-activated cell sorting, and tried to detect the *Nrf2* and *Keap1* genes. In the absence of nerve crush (NC), the number of RGCs in Nrf2 KO mice was almost same as that in WT mice. 1-(2-cyano-3-, 12-dioxooleana-1, 9 (11)-dien-28-oyl) imidazole (CDDO-Im), an Nrf2 activator, prevented NC-induced loss of RGCs in WT mice. Seven days after NC, without treatment, the number of RGCs in Nrf2 KO mice was significantly lower than in WT mice. In addition, after CDDO-Im treatment, quantitative RT-PCR showed increased expression of antioxidant and phase II detoxifying enzymes. These results suggest that up-regulation of Nrf2 signaling after CDDO-Im treatment may be a novel therapeutic strategy for the protection of RGCs, especially in glaucoma.

Keywords: glaucoma, neuroprotection, Nrf2, oxidative stress, retinal ganglion cell.

J. Neurochem. (2013) **127**, 669–680.

Glaucoma is well known to be one of the world's major causes of secondary blindness (Quigley 1996). It is thought that the ultimate cause of vision loss in this disease is retinal ganglion cell (RGC) apoptosis (Yücel *et al.* 2003). Therefore, the neuroprotection of RGCs has recently drawn attention as a new approach to glaucoma therapy.

Several hypotheses have been proposed for potential mechanisms triggering RGC death in glaucoma, including compromised blood flow at the optic nerve (Hayreh 1997; Kerr *et al.* 1998), nitric oxide–induced injury to the optic nerve (Neufeld *et al.* 1999; Shareef *et al.* 1999; Liu and Neufeld 2001), and glutamate excitotoxicity (Vorwerk *et al.* 1999; Sullivan *et al.* 2006; Seki and Lipton 2008). In addition to these primary mechanisms, some studies have provided evidence that oxidative stress contributes to the degeneration of RGCs in glaucoma (Izzotti *et al.* 2006; Engin *et al.* 2010; Ferreira *et al.* 2010; Bagnis *et al.* 2012). However, the precise nature of RGC damage caused by oxidative stress remains unclear.

NF-E2-related factor2 (Nrf2) is a transcription factor that is activated by oxidative stress and the presence of electrophiles, controlling hundreds of detoxifying and antioxidant

Received April 22, 2013; revised manuscript received May 28, 2013; accepted May 29, 2013.

Address correspondence and reprint requests to Toru Nakazawa, Department of Ophthalmology, Tohoku University Graduate School of Medicine, 1-1 Seiryo, Aoba, Sendai, Miyagi, 980-8574, Japan.
E-mail: ntoru@oph.med.tohoku.ac.jp

Abbreviations used: 4Di-10ASP, *N*-4-[4-didecylaminostryryl]-*N*-methyl-pyridinium iodide; ARE, antioxidant response elements; CDDO-Im, 1-(2-cyano-3-, 12-dioxooleana-1, 9 (11)-dien-28-oyl) imidazole; DAB, diaminobenzidine; FACS, fluorescence-activated cell sorting; FG, fluorogold; GCL, ganglion cell layer; HBSS, Hank's buffered saline solution; HNE, hydroxynonenal; IOP, intraocular pressure; Keap1, Kelch-like ECH associated protein 1; NC, nerve crush; Nrf2 KO, Nrf2 deficient mice; Nrf2, NF-E2 related factor 2; NTG, normal tension glaucoma; OAG, open angle glaucoma; OHdG, hydroxy-2′-deoxyguanosine; PVDF, polyvinylidene fluoride; QPCR, quantitative RT-PCR; RGC, retinal ganglion cell; ROS, reactive oxygen species; RT-PCR, reverse transcription PCR; TBARS, thiobarbituric acid reactive substances; WT, wild type.

genes. Under basal conditions, the cytosolic regulatory protein Kelch-like ECH associated protein 1 (Keap1) sequesters Nrf2 in the cytoplasm. Upon exposure to oxidative or electrophilic stress, Nrf2 is released from Keap1 repression and translocates to the nucleus where it heterodimerizes with small Maf proteins to enhance transcription of the target genes via antioxidant response elements in the promoters (Itoh *et al.* 1997). In Nrf2 knockout (Nrf2 KO) mice, induction of antioxidant response elements-dependent cytoprotective genes is severely impaired, making them susceptible to a variety of pharmacological and environmental toxicants (Aoki *et al.* 2001; Enomoto *et al.* 2001; Osburn and Kensler 2008; Uno *et al.* 2010). This makes Nrf2 KO mice useful to investigate the role of oxidative stress in the pathological condition of eye diseases (Nagai *et al.* 2009; Zhao *et al.* 2011; Shanab *et al.* 2012).

Normal tension glaucoma (NTG), in which patients have normal intraocular pressure, is an important subset of open angle glaucoma. NTG is also more prevalent in the Asian population (Iwase *et al.* 2004). Interestingly, both glutamate excitotoxicity and oxidative stress are involved in RGC death in glutamate transporter KO mice, a model of NTG (Harada *et al.* 2007). Our present data was derived from experiments based on nerve crush (NC), which is a commonly used model of axonal injury. It provides insight into the mechanisms involved in the death of the RGCs by providing a precise, short-term synchronous insult to the axons. This results in secondary RGC apoptotic cell death that resembles glaucoma. Therefore, NC should be a good model for the investigation of NTG.

Nrf2 has shown strong potential to protect against a broad range of diseases associated with oxidative stress (Clements *et al.* 2006; Padmanabhan *et al.* 2006; Satoh *et al.* 2006; Singh *et al.* 2006). However, its role in the glaucoma model remains unclear. In this study, we hypothesize that Nrf2 protects retinal neurons from oxidative stress. To elucidate this role, we investigated the functions of Nrf2 in NC-induced RGC death. We also tested whether enhancing Nrf2 signaling with the extremely potent synthetic triterpenoid activator 1-(2-cyano-3,12-dioxooleana-1,9(11)-dien-28-pyl)imidazole (CDDO-Im) (Liby *et al.* 2005), protects against oxidative stress-induced RGC death. In short, we explored whether CDDO-Im had a neuroprotective effect against RGC damage.

Method

Animals

Male Nrf2 KO mice (C57BL/6J mouse background, 10–12 weeks old, 20–25 g: The Nrf2 KO mice were bred and maintained at our institution, and were kindly provided by Dr. Masayuki Yamamoto and Dr. Keiko Taguchi) and age- and sex-matched C57BL/6J mice were housed in covered cages. The mice were genotyped for Nrf2 status with PCR amplification of genomic DNA extracted from tail snips (Aoki *et al.* 2007). PCR amplification was performed using three different primers: 5′-TGGACGGGACTATTGAAGGCTG-3′ (sense for both genotypes), 5′-GCCGCCTTTTCAGTAGATGGA GG-3′ (antisense for wild type), and 5′-GCGGATTGACCGTAA TGGGATAGG-3′ (antisense for LacZ). All animals were maintained and handled in accordance with the guidelines of the Association for Research in Vision and Ophthalmology Statement for the Use of Animals in Ophthalmic and Vision Research and the guidelines from the declaration of Helsinki and the Guiding Principles in the Care and Use of Animals. All experimental procedures described in this study were approved by the Ethics Committee for Animal Experiments at Tohoku University Graduate School of Medicine, and were performed according to the National Institutes of Health guidelines for the care and use of laboratory animals.

Immunohistochemistry

The eyes were enucleated and washed, then fixed in 4% paraformaldehyde overnight at 4°C, immersed in a 20% sucrose solution, and embedded in an optimal cutting temperature compound (Sakura Finetechnical Co. Ltd., Tokyo, Japan). Transverse 10 μm-thick cryostat sections were cut and placed onto slides (MAS COAT; Matsunami Glass Ind. Ltd., Osaka, Japan). Immunohistochemical staining has been described previously (Inokuchi *et al.* 2009). Briefly, the tissue sections were washed in 0.01 M phosphate-buffered saline (PBS) for 10 min. We used 8-hydroxy-2′-deoxyguanosine (OHdG) and 4-hydroxynonenal (HNE) mouse monoclonal antibody (Japan Institute for the Control of Aging, Shizuoka, Japan). When 8-OHdG was used, the primary antibody was incubated at 4°C overnight. With 4-HNE, the tissue sections were incubated with the antibody for 1 h. Next, endogenous peroxidase was quenched by treating the sections with 3% hydrogen peroxide in absolute methanol for 10 min. The sections were washed, and then incubated with biotinylated anti-mouse IgG. They were subsequently incubated with the avidin-biotin-peroxidase complex for 30 min, and were then developed using diaminobenzidine peroxidase substrate for 1 min.

Thiobarbituric acid reactive substances

The levels of thiobarbituric acid reactive substances (TBARS) in the retinas were analyzed (Ferreira *et al.* 2010; Salido *et al.* 2012). Each retina was homogenized in 56 mM potassium chloride buffer and centrifuged at 20 000 g for 10 min at 4°C. The sediment was used for analysis. It was mixed with 8.1% sodium dodecyl sulfate, 0.8% 2-Thiobarbituric acid and 20% acetic acid. The samples were heated for 1 h at 100°C. After they had cooled, they were measured with fluorescence at an excitation wavelength of 530 nm and an emission wavelength of 550 nm with a Kinetic Microplate Reader (Molecular Devices, Sunnyvale, CA, USA). The results were normalized to protein concentration.

Oxidative stress and mitochondrial proteins

Retrograde labeling was performed as described below. Seven days afterwards, optic nerve surgery was performed, and after seven more days, the retinas were harvested. The retinas were then washed with Dulbecco's phosphate-buffered saline and stained with both 500 nM MitoTracker Deep Red FM (Invitrogen, Carlsbad, CA, USA) and 5 μM CellRox Green Reagent (Invitrogen) at 4°C for 2 h. After washes with Dulbecco's phosphate-buffered saline, the retinas were fixed with 4% paraformaldehyde at 4°C for 2 h, and were then flat mounted onto glass slides. Imaging was performed with a confocal

laser-scanning microscope (LSM5 PASCAL; Carl Zeiss, Jena, Germany).

Retrograde labeling and counting of RGC

Retrograde labeling was performed as described in our previous research (Nakazawa *et al.* 2007b; Ryu *et al.* 2012). Briefly, RGCs were retrogradely labeled with a fluorescent tracer, Fluoro-gold (FG; Fluorochrome, LLC, Denver, CO, USA), or carbocyanine dye, *N*-4-[4-didecylaminostryryl]-*N*-methyl-pyridinium iodide (4Di-10ASP; Molecular Probes, Eugene, OR, USA). 1 μL of 2% aqueous FG in 1% dimethylsulfoxide or of 3% 4Di-10ASP in dimethylformamide was injected into the superior colliculus with a 32 G needle.

Seven days after FG labeling, a NC procedure was performed in the right eye only. Seven days after NC, the mice were killed and their complete retinas were placed on glass slides with the ganglion cell layer facing up. Vectashield mounting medium (Vector Laboratories, Burlingame, CA, USA) and cover glass were applied. RGC density was determined by counting tracer-labeled RGCs in 12 distinct areas under the microscope, as previously described (Nakazawa *et al.* 2002a,b).

RGC purification

Seven days after retrograde labeling, the 4Di-10ASP-labeled mice were killed. The retinas were rapidly dissected, incubated in a digestion solution containing papain (10 U/mL; Worthington-Biochemical Co., Lakewood, NJ, USA) and L-cysteine (0.3 mg/mL; Sigma-Aldrich, St Louis, MO, USA) in Hank's Buffered Saline Solution (Invitrogen), and incubated at 37°C for 15 min (CO_2 incubator). The retinas were rinsed twice in Hank's Buffered Saline Solution, and dissociated in Neurobasal A medium containing a B27 supplement (NBA/B27 AO+; Invitrogen). The dissociated cells were passed through a cell strainer (40 μm nylon net; BD-Falcon, Bedford, MA, USA), cooled to 4°C, and immediately sorted using a fluorescence-activated cell sorting (FACS) Aria II (Becton-Dickinson, San Jose, CA, USA). A 585/42 filter was used to detect the 4Di-10ASP-labeled RGCs. The cells were sorted directly into 350 μL of buffer RLT Plus (RNeasy kit; Qiagen, Valencia, CA, USA) with 1% β-mercaptoethanol, frozen immediately, and stored at −80°C until further use. The sorted cells were placed in serum-free media without growth factors, and the yield, purity, and viability of the RGCs were determined after 2 h in culture. To determine the immunocytochemistry of the RGC marker Thy1, retinal cells were incubated, on ice, with FITC-conjugated anti-Thy1 antibody (12.5 μg/mL; BD Biosciences, San Diego, CA, USA) for 30 min. They were then treated with isotype-matched nonspecific IgG antibodies, which were used as isotype controls. Finally, the sorted RGCs were re-suspended in medium and observed with a microscope. Independent sets of samples were prepared, each containing 6000 RGCs, for each experimental condition, namely, RGCs subjected to NC injury and normal controls. Total RNA was extracted from FACS-purified RGCs using RNeasy Micro Kit (Qiagen), according to the manufacturer's protocol. The RNA was then concentrated using RNeasy MinElute Spin columns (Qiagen).

Immunoblot analysis

One day after nerve crush, the retinas were rinsed in PBS for protein expression analysis. Nuclear extract was isolated using NE-PER Nuclear and Cytoplasmic Extraction Reagents (Thermo Scientific, Rockford, IL, USA) according to the manufacturer's instructions. The nuclear and cytoplasmic fractions were first treated with SDS sample buffer, and then heated to 100°C, for 5 min. Protein concentrations were measured using the bicinchoninic acid protein assay kit (Thermo Scientific). Each sample was separated with sodium dodecyl sulfate–polyacrylamide gel electrophoresis and electroblotted onto a polyvinylidene fluoride membrane (Millipore, Bedford, MA, USA). After non-specific binding had been blocked with 4% BlockAce (Yukijirushi, Sapporo, Japan), the membranes were incubated at 4°C overnight with a rabbit monoclonal antibody against Nrf2 (1 : 500; Cell signaling Technology, Beverly, MA, USA), β-actin (1 : 1000; Sigma-Aldrich) and TATA binding protein (1 : 500; Cell signaling Technology). The membranes were then incubated with a horseradish peroxidase-conjugated rabbit immunoglobulin secondary antibody for 1 h. The signals were visualized with chemiluminescence (ECL blotting Analysis System; Amersham, Arlington Heights, IL, USA) and measured in Image Lab statistical software (Bio-Rad, Hercules, CA, USA). Cytoplasmic fractions were normalized to β–actin and nuclear fractions were normalized to TATA binding protein.

Reverse transcription PCR with retinas from Nrf2 KO mice

Total RNA extraction and RT-PCR were performed as previously reported, with minor modifications (Nakazawa *et al.* 2006a). RT-PCR was performed with RNA from the retinas of Nrf2 KO and wild-type (WT) mice. The RT-PCR thermocycle program (PCR Thermal Cycler MP; Takara Bio, Shiga, Japan) consisted of denaturation at 94°C for 4 min, followed by 27 cycles of denaturation at 94°C for 30 s, annealing at 61°C for 30 s, and an extension at 72°C for 30 s. The final extension was at 72°C for 10 min. The primer sets used in this study were as follows (*Nrf2*: F: TGCCCCTCATCAGGCCCAGT; R: GCTCGGCTGGGACTCG TGTT, *Keap1*: F: GGTGGCGCGCTGTGCTTAGT; R: TGCTG GCTCAGGCGAAGCTC, and *Gapdh*: F: TCTGACGTGCCGCCT GGAGA; R: GGGGTGGGTGGTCCAGGGTT). The expected product length was 588 bp (*Nrf2*), 340 bp (*Keap1*), and 299 bp (*Gapdh*).

Quantitative RT-PCR

Quantitative RT-PCR (QPCR) was performed as previously described (Nakazawa *et al.* 2006b, 2007a,b) with minor modifications. The retinas were sampled and immediately sunk in RNA stabilization reagent (RNase later sample and assay technology; Qiagen). Total RNA was extracted from the retinas and purified RGCs (6000 RGCs) as described above with the RNeasy Micro Kit (Qiagen) and cDNA was synthesized with SuperScript III reverse transcriptase (Invitrogen). QPCR was performed with a 7500 Fast Real Time PCR System (Applied Biosystems, Foster city, CA, USA) by TaqMan Gene Expression Assays (Applied Biosystems). TaqMan Fast Universal PCR master mix (Applied Biosystems) was used for QPCR to quantify mRNA levels with commercially available TaqMan probes for *Thy1* (Mm00493682_g1), *Nrf2* (Mm00477786_m1), *Keap1* (Mm00497268_m1), *Nqo1* (Mm00500821_m1), *Ho-1* (Mm00516007_m1), *Gsta4* (Mm00494803_m1), *Txnrd* (Mm00443675_m1), *Gclm* (Mm00514997_m1), *Gclc* (Mm00802657_g1), and *Gapdh* (Mm99999915_g1). The mRNA levels were normalized to *Gapdh* as an internal control.

Gene expression analysis

To assess the effects of CDDO-Im (obtained from Mochida Pharmaceuticals) on NC-induced RGC death, we initially administered different doses to three groups of mice for 3 days, via gavage: 1, 3, or 10 μmol/kg body weight (dissolved in 10% dimethylsulfoxide, 10% Cremophor-EL, PBS). However, CDDO-Im at these doses did not result in an increase in the expression of Nrf2-regulated cytoprotective genes, such as *Nqo1*, *Ho-1*, *Gclc*, *Gclm*, *Gsta4*, and *Txnrd* (data not shown). Therefore, we added a new group of mice, treated with CDDO-Im at 30 μmol/kg body weight. All groups were administered CDDO-Im or vehicle via gavage, and were killed 6 h after the last dose. We then removed the retinas and immediately placed them in RNA later for RNA purification and gene expression measurements, as described above.

Statistical analysis

All data were expressed as mean ± SD. The values were processed for statistical analysis, (Mann–Whitney *U*-test) followed by a two-tailed Student's *t*-test. Differences were considered statistically significant at $p < 0.05$.

Results

The expression of mRNA and retinal reactive oxygen species increase after NC

RT-PCR analysis revealed that *Nrf2* (588 bp) and *Keap1* (340 bp) were expressed in the retinas of WT mice, but that in the retinas of Nrf2 KO mice, Nrf2 mRNA had been completely eliminated (Fig. 1a). To confirm antioxidative effects in the mouse retina after NC, 8-OHdG and 4-HNE were measured using the immunostaining technique. In DNA, 8-OHdG is a well-known marker for oxidative stress-induced damage. To assess cellular DNA damage, we performed IHC for the anti-8-OHdG antibody. Cells positive for 8-OHdG were observed in the ganglion cell layer (GCL) 7 days after NC, while almost none were seen in retinas without NC (Fig. 1b). We next performed IHC for the 4-HNE antibody, which is a by-product of lipid peroxidation. Cells positive for 4-HNE were observed in the GCL of the retina after NC, but almost none were seen in

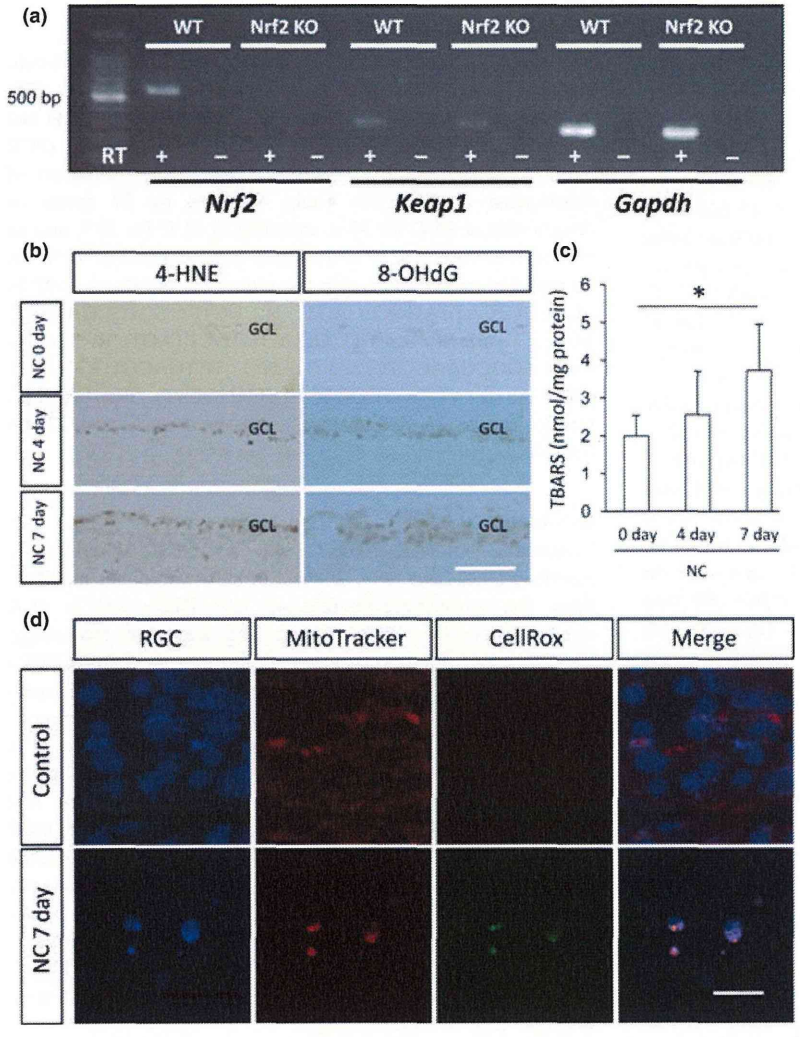

Fig. 1 (a) RT-PCR of the retina. RT-PCR analysis confirmed the presence and absence of *Nrf2* mRNA in the retina of wild-type and Nrf2 deficient mice, respectively. (b) Representative immunohistochemistry for 8-OHdG and 4-HNE-modified proteins in the retina after nerve crush. (c) Thiobarbituric acid reactive substances values of retina ($n = 6$ in each group). *$p < 0.05$. (d) Confocal images of reactive oxygen species and mitochondria. Blue, Fluoro-gold labeled retinal ganglion cell, red, Mito Tracker, green, CellRox. Scale bar 20 μm.

the GCL of retinas without NC (Fig. 1b). To confirm the overproduction of reactive oxygen species (ROS) in the retinas after NC, we checked TBARS values. The TBARS level was assessed in the retinas after NC as an index of lipid peroxidation. Levels were significantly higher 7 days after NC ($p < 0.05$; Fig. 1c). Compared to the control group, however, no significant change was observed in the levels of TBARS 4 days after NC. Moreover, we investigated the expression of ROS in the mitochondria of the RGCs after NC (Fig. 1d). To evaluate ROS production, we used CellROX Deep Green reagent. ROS positive cells (green) were not observed in RGCs without NC. However, at 7 days after NC, a significant number of ROS positive cells were present in the RGCs. Some RGCs, both with and without NC, were also stained with MitoTracker Red dye, a commercially available mitochondrial indicator. Co-localization of the ROS positive cells with MitoTracker was seen in RGCs 7 days after NC.

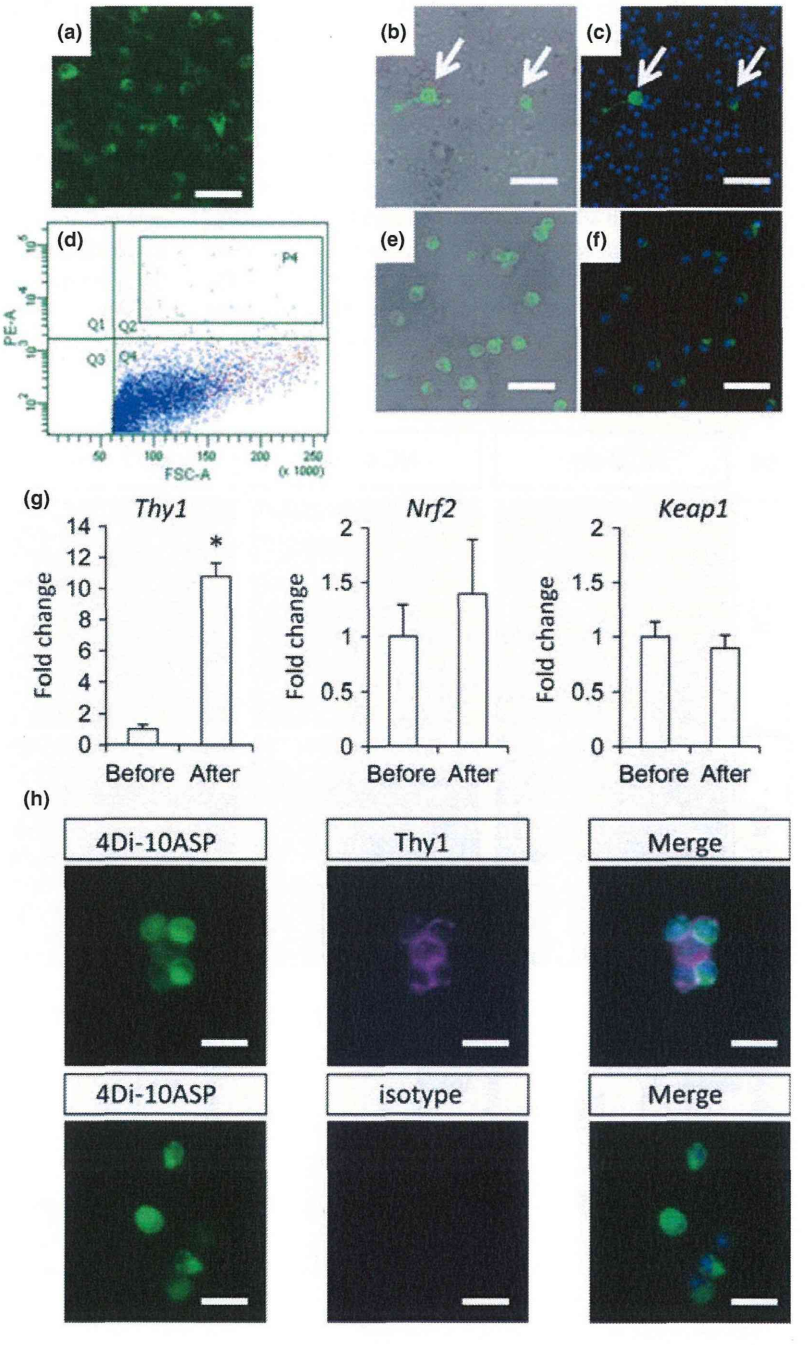

Fig. 2 Retinal ganglion cell (RGC) purification using fluorescence-activated cell sorting (FACS) from dissociated retinas retrogradely labeled with *N*-4-[4-didecylaminostryryl]-*N*-methyl-pyridinium iodide (4Di-10ASP). (a) Representative photograph of a flat-mount retina. The RGCs were labeled with 4Di-10ASP (green). (b, c) Representative photographs of dissociated retinal cells before sorting. (d) Analysis of retinal cells by FACS. (e, f) Representative photographs of large cells with high fluorescence selected for sorting. Scale bar 50 μm. (g) quantitative RT-PCR results showing the quality of cell purification. We assessed the relative abundance of *Thy1*, the marker gene for RGCs. *Nrf2* and *Keap1* were also detected in the RGCs. $*p < 0.05$. (h) Representative immunocytochemistry photographs of RGCs after sorting. Thy1 was mainly expressed in sorted RGCs. Nuclei were labeled with DAPI (blue). Green represents 4Di-10ASP labeled RGCs. Purple represents Thy1. Scale bar 20 μm.

Isolation of RGCs by fluorescence-activated cell sorting

Because RGCs represent only a small percentage of the total cell population in the retina, it was necessary to purify these cells to investigate changes in gene expression in them. The ratio of 4Di-10ASP$^+$ RGCs in a sample of dissociated retinal cells before sorting was only 0.2% (Fig. 2b and c). High purification was achieved using FACS, taking advantage of the fact that RGCs are the only cells in the retina that are marked when 4Di-10ASP is injected into the superior colliculus. RGCs were retrogradely labeled with 4Di-10ASP 7 days after NC (Fig. 2a). FACS analysis demonstrated that before sorting, the population of large and highly fluorescent cells in the dissociated retina was relatively small (Fig. 2d). Large cells with high fluorescence were selected for sorting. After sorting, the proportion of these cells had increased (Figs. 2e and f). The data showed that the ratio of 4Di-10ASP$^+$ RGCs to 4′-6-diamino-2-phenylindole (DAPI$^+$) cells following cell sorting was 96.4%, a high level of RGC purity. In addition, we used QPCR to assess the relative abundance of *Thy1*, the marker gene for RGCs, in the purified cells. We found *Thy1* to be over 10 times more abundant than before sorting (Fig. 2g). Finally, we examined the expression of *Nrf2* and *Keap1* in the purified RGCs with QPCR, and found that they were detectable (Fig. 2g). To confirm the number of collected cells from the flowcytometry analysis, we stained the cells with an RGC marker, such as Thy1 (Fig. 2h). Thy1 was detected in the sorted RGCs, but not in the isotype controls. This immunocytochemistry result clearly indicated that the collected cells were RGCs.

The role of Nrf2 in RGC death following NC

To investigate the neuroprotective effect of Nrf2 after NC, we first performed NC on WT and Nrf2 KO mice, and then assessed the density of surviving RGCs 4 and 7 days later (Fig. 3a and b). Before undergoing NC, there was no significant difference in the density of FG-labeled RGCs in WT (3815 ± 430 cells/mm^2) and Nrf2 KO mice (3846 ± 468 cells/mm^2). Four days following NC, there was still no significant difference in the density of FG-labeled RGCs in WT (3022 ± 473 cells/mm^2) and Nrf2 KO mice (2503 ± 634 cells/mm^2). However, 7 days following NC, the density of FG-labeled RGCs had decreased significantly in the Nrf2 KO mice (313 ± 123 cells/mm^2) compared to the WT mice (692 ± 88 cells/mm^2, $p < 0.01$).

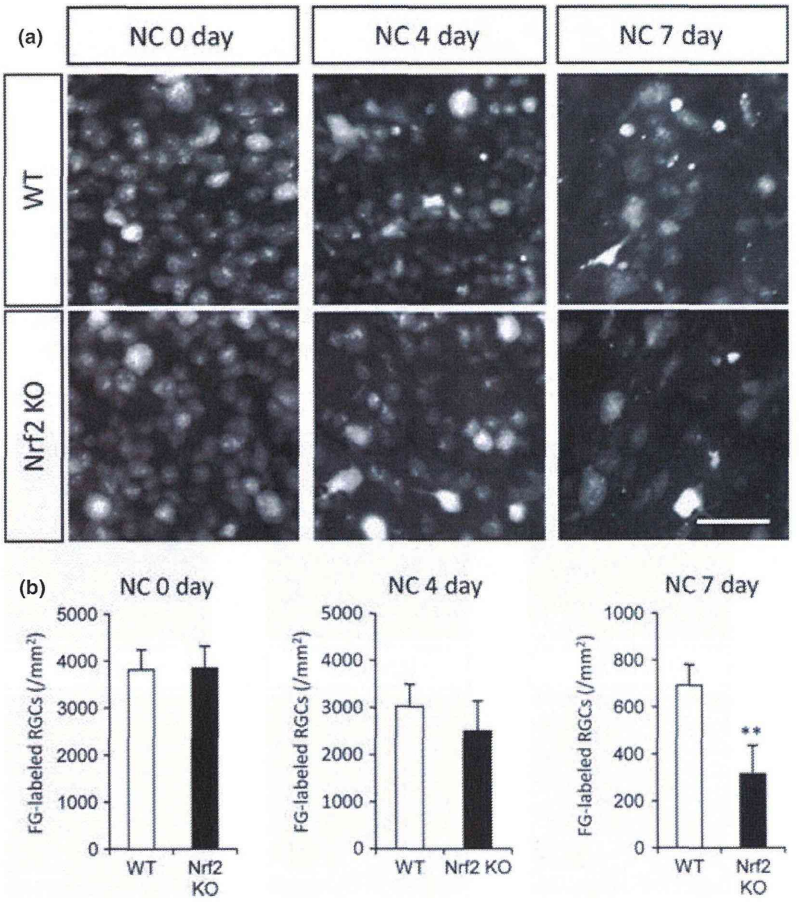

Fig. 3 Vulnerability of Nrf2 deficient mice to nerve crush (NC) injury. (a) Representative photographs of retinal ganglion cell (RGC)s in flat mounted retinas. Scale bar 50 μm. (b) Quantitative data on the density of RGCs after NC injury (n = 5–6 in each group). $^{**}p < 0.01$.

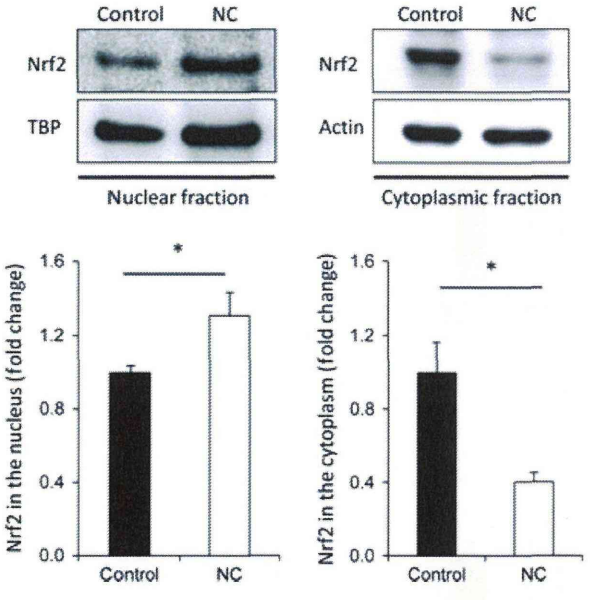

Fig. 4 We extracted nuclear and cytoplasmic fractions from the retinas. TATA binding protein (TBP) and β-actin (Actin) were used as internal controls for the nuclear and cytoplasmic fractions. Bar graphs show cumulative data for immunoblotting band densities (n = 3 in each group).

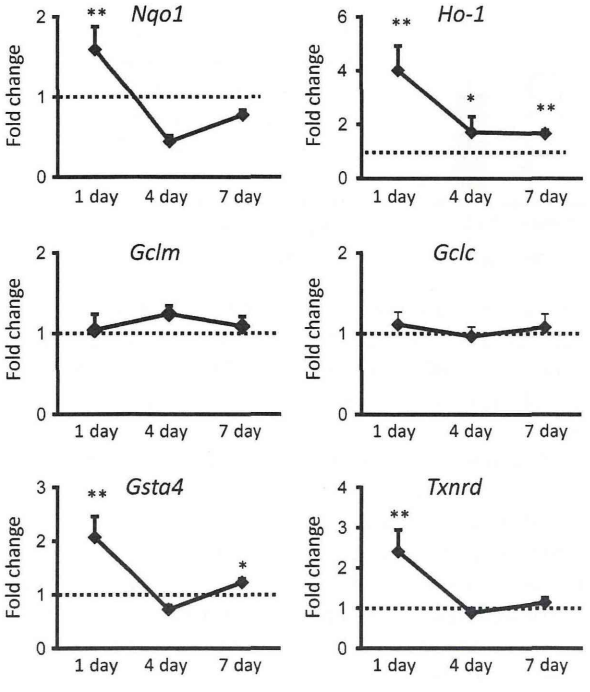

Fig. 5 Changes in retina gene expression. mRNA expression of antioxidant enzymes in the retina increased at 1, 4 and 7 days after nerve crush (n = 3–6 in each group). The graphs show the ratio of expression to sham-operated wild-type mice. *$p < 0.05$, **$p < 0.01$.

Nuclear accumulation of Nrf2 1 day after NC

We investigated the role of Nrf2 in axonal damage-induced RGC death, and were able to detect Nrf2 1 day after NC. Immunoblot analysis showed that NC promoted nuclear accumulation of Nrf2 ($p < 0.05$; Fig. 4). We confirmed the efficacy of cell fractionation by using anti-TATA binding protein and anti-β-actin antibodies as loading controls to detect nuclear and cytoplasmic proteins. Our results showed that Nrf2 immediately translocates into the nucleus from the cytoplasm after NC.

The gene expression pattern of Nrf2-related factors after NC

We examined changes in gene expression in the extracted retinas at 1, 4 and 7 days after NC (Fig. 5). The results were normalized to expression levels in retinas that had not undergone NC. One day after NC, we found that expression of *Nqo1*, *Ho-1*, *Gsta4,* and *Txnrd* had increased ($p < 0.01$). Four days after NC, *Ho-1* continued to have a high level of expression ($p < 0.05$). Seven days after NC, moreover, expression of *Ho-1* had increased still further, while expression of *Gsta4* had also risen ($p < 0.01$, $p < 0.05$). However, *Gclm* and *Gclc*, enzymes that directly regulate levels of glutathione, did not change their expression after NC.

CDDO-Im induces phase II and antioxidant genes

To test whether CDDO-Im, a potent activator of Nrf2, influences Nrf2 in the eye, WT and Nrf2 KO mice were treated with CDDO-Im daily for 3 days. Following this, phase II and antioxidant gene expression was measured in the retina. A statistically significant induction of these genes occurred in the retina following a dose of 30 μmol/kg (data not shown). CDDO-Im induced the expression of many genes in WT mice that were not induced in Nrf2 KO mice, such as *Nqo1*, *Ho-1*, *Gclm*, *Gclc*, *Gsta4*, and *Txnrd*, indicating that these responses are Nrf2 dependent (Fig. 6). Enzyme levels for the WT and Nrf2 KO mice were both set at 1 for the vehicle groups only to more easily show relative changes. The absolute mRNA levels of the vehicle-group Nrf2 KO mice were not the same as of the vehicle-group WT mice. In fact, mRNA levels of antioxidant enzymes were lower in the Nrf2 KO mice than in the WT mice.

Oxidative stress-induced RGC death inhibition with CDDO-Im

We investigated the activation of Nrf2 by CDDO-Im, and the possibility of a preventive effect against oxidative stress-induced RGC death. Seven days after NC, the density of FG-labeled RGCs in WT mice treated with CDDO-Im was significantly higher than in those treated with vehicle (1337 ± 219 cells/mm^2 and 819 ± 185 cells/mm^2, respectively, $p < 0.01$; Fig. 7c). In contrast, Nrf2 KO mice treated with CDDO-Im (490 ± 77 cells/mm^2) showed no difference from those treated with vehicle (450 ± 92 cells/mm^2) 7 days after NC.

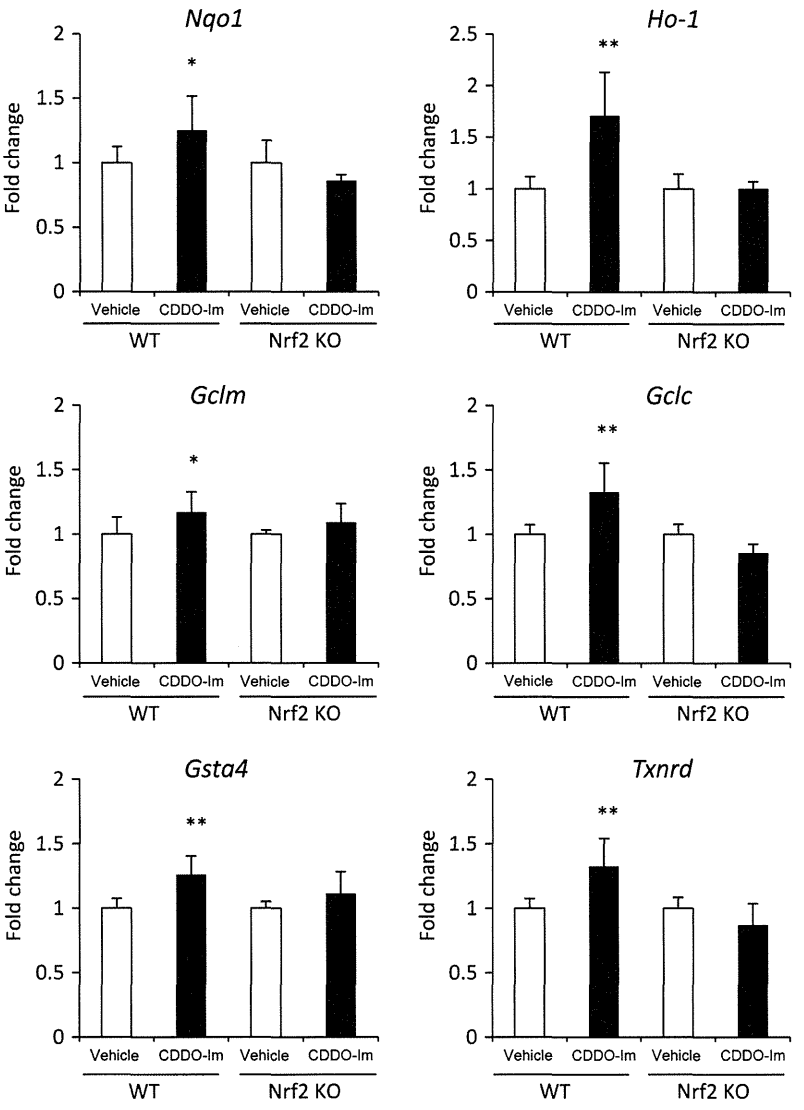

Fig. 6 Changes in mRNA levels measured by quantitative RT-PCR in mice retinas after treatment with 1-(2-cyano-3,12-dioxooleana-1,9(11)-dien-28-pyl)imidazole (CDDO-Im). Wild-type (WT) and Nrf2 deficient (Nrf2 KO) mice were administered CDDO-Im or vehicle at 1 day intervals over the course of 3 days. Open columns: WT or Nrf2 KO mice treated with vehicle, and solid columns: WT or Nrf2 KO mice treated with CDDO-Im (30 μmol/kg; $n = 4$–6 in each group). $^{*}p < 0.05$, $^{**}p < 0.01$.

Discussion

The results of this study suggest that the *Nrf2* gene is an important factor in protecting RGCs from axonal damage-induced RGCs death because of oxidative stress conditions. We compared the density of FG-labeled RGCs in WT and Nrf2 KO mice both with 7 days after NC or without NC. We observed that there was no difference of FG-labeled RGCs without NC, while significantly fewer FG-labeled RGCs in the Nrf2 KO mice than in the WT mice. This suggests that Nrf2 deficiency augments NC-induced RGC death. In contrast, CDDO-Im, an extremely potent activator of Nrf2, also demonstrated a neuroprotective effect against NC-induced RGC death *in vivo*. These data strongly suggest that Nrf2 has a neuroprotective effect on RGCs.

Oxidative stress is implicated in neuronal cell death in many neurodegenerative diseases, such as Alzheimer's disease (Ramamoorthy *et al.* 2012), amyotrophic lateral sclerosis (Lee *et al.* 2009), and Parkinson's disease (Clements *et al.* 2006; Choi *et al.* 2012). Nrf2 activation has been demonstrated to be a viable therapeutic target for the prevention of chronic neurodegeneration (Clements *et al.* 2006; Vargas *et al.* 2008). Our results clearly and strongly suggest that glaucoma should also be considered a chronic neurodegenerative disease associated with oxidative stress. Furthermore, we believe we have shown that activation of the Nrf2 pathway has the potential to be a new neuroprotective treatment for glaucoma, particularly normal tension glaucoma (the main type of glaucoma in Asian countries) (Iwase *et al.* 2004).

As RGCs represent only a small fraction of the total retinal cell population, many important responses in RGCs are easily masked. In an effort to identify changes more specific to RGCs, Fischer *et al.* studied gene expression in individual

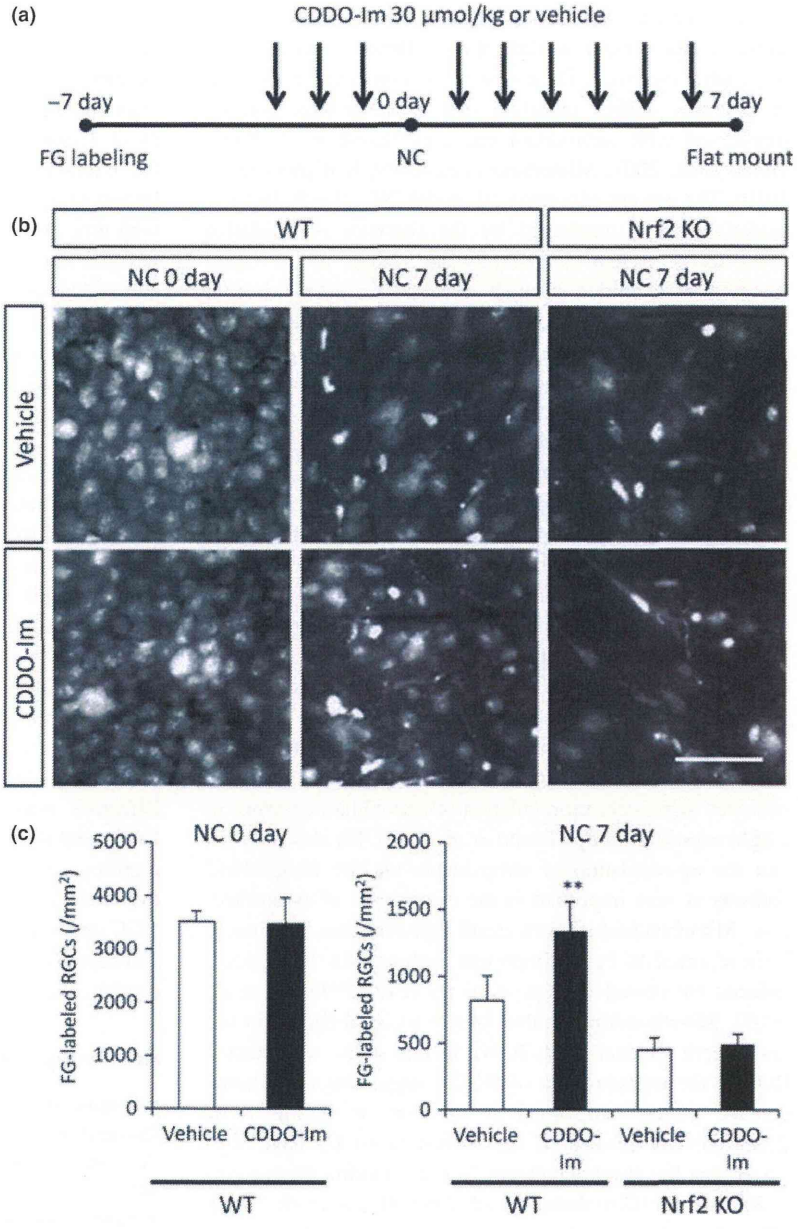

Fig. 7 Effects of activation of Nrf2 by 1-(2-cyano-3,12-dioxooleana-1,9(11)-dien-28-pyl)imidazole (CDDO-Im) on retinal ganglion cell (RGC) death. (a) Protocol for evaluating CDDO-Im. The arrows indicate the days gavage of CDDO-Im was performed: CDDO-Im at 30 μmol/kg body weight every 24 h before nerve crush (NC) for 3 days, and after NC for six more days. (b) Representative photographs of RGCs in flat mounted retinas. Scale bar 50 μm. (c) Quantitative data on the density of RGCs after NC injury with and without CDDO-Im treatment (30 μmol/kg; $n = 4$–6 in each group). $^{**}p < 0.01$.

rat RGCs sorted with FACS (Fischer *et al.* 2004). In this study, we showed that adult primary neurons could also be isolated in mice. We modified a FACS-based cell purification technique and successfully used it to isolate RGCs from the retina. RGCs normally represent less than 0.5% of cells in the retina. The combination of sorting cells by retrograde fluorescent label and cell size allowed us to obtain a high purity of RGCs in a simple one-step procedure. By isolating RGCs, we were able to confirm that *Nrf2* and *Keap1* were expressed not only in the retinas but also in the RGCs of mice. These data may suggest that the RGC purification technique would be necessary and helpful for exploring the glaucoma pathogenesis because RGC was small population in the retinal cells.

Previous reports showed that oxidative stress could induce the apoptosis of RGCs (Maher and Hanneken 2005a,b; Inomata *et al.* 2006). Recently we also demonstrated that Nrf2 KO mice were susceptible for hyperglycemia-induced RGC death (Shanab *et al.* 2012), where the oxidative stress and subsequent intracellular calcium influx has pivotal roles in RGC death. ROS play a beneficial role in cell signaling, but their uncontrolled production can lead to cell damage through necrosis or apoptosis. ROS, which include free radicals such as superoxide anions, hydroxyl radicals, lipid